Title

Supplementing Shear Wave Velocity Profile Database with Microtremor-Based H/V Spectral Ratios

Authors
Gospe, Tatiana
Zimmaro, Paolu
Wang, Pengfei
et al.

Publication Date
2020-06-19

Peer reviewed

SUPPLEMENTING SHEAR WAVE VELOCITY PROFILE DATABASE WITH MICROTREMOR-BASED H/V SPECTRAL RATIOS

T. Gospe[1], P. Zimmaro[2], P. Wang[3], T. Buckreis[4], S.K. Ahdi[5], A.K. Yong[6], S.J. Brandenberg[7], J.P. Stewart[8]

[1] *Graduate Student Researcher, University of California, Los Angeles, tbgospe@g.ucla.edu*
[2] *Project Scientist and Lecturer, University of California, Los Angeles, pzimmaro@ucla.edu*
[3] *Graduate Student Researcher, University of California, Los Angeles, wltcwpf@g.ucla.edu*
[4] *Graduate Student Researcher, University of California, Los Angeles, tristan.buckreis@live.com*
[5] *Associate, Exponent, Inc.; Lecturer, University of California, Los Angeles, sahdi@ucla.edu*
[6] *Research Geophysicist, United States Geological Survey, Pasadena, yong@usgs.gov*
[7] *Professor, University of California, Los Angeles, sjbrandenberg@ucla.edu*
[8] *Professor, University of California, Los Angeles, jstewart@seas.ucla.edu*

Abstract

Frequency-dependent horizontal-to-vertical spectral ratios (HVSR) can provide information on one or more site resonant frequencies and relative levels of amplification at those frequencies. Such information is potentially useful for predicting site amplification but is not present in site databases that have been developed over the last 15–20 years for the Next-Generation Attenuation (NGA) projects, which instead use the time-averaged shear-wave velocity (V_S) in the upper 30 m of the site (V_{S30}) as the primary site parameter and are supplemented with basin depth terms where available.

In order for HVSR-based parameters to be used in future versions of site databases, a publicly accessible repository of this information is needed. We adapt a relational database developed to archive and disseminate V_S data to also include HVSR. Our intent with the database is to provide relevant HVSR data and supporting metadata, but not parameters derived from the data. We consider the relevant data to be the frequency-dependent HVSR, where the horizontal is taken as the median component and as a function of horizontal azimuth (referred to as *polar plots*). Relevant metadata includes site location information, details about the equipment used to make the measurements, and processing details related to windowing, anti-trigger routines, and filtering. We describe the database schema developed to organize and present this information.

The relational database stores HVSR data, but not site parameters derived from the data. Site parameters of potential interest for modeling purposes include: (1) a binary variable indicating whether an HVSR plot contains a peak; (2) one or more peak frequencies; (3) peak amplitudes; and (4) peak widths. We describe and illustrate analysis routines to derive these parameters that are implemented in Python on a Jupyter Notebook enabled by DesignSafe-CI. These routines interact with the database via cloud computing, but are not directly part of the database.

Keywords: horizontal-to-vertical spectral ratios, resonant frequencies, site response, relational database

1. Introduction

Seismic site response is influenced by several factors, including: resonance, nonlinearity, amplification due to impedance contrasts, and amplification related to wave propagation in sedimentary basins. Ground-motion models predict site response conditioned on relatively simple site parameters such as the time-averaged shear wave velocity (V_S) to 30 m depth (V_{S30}) and depth to the 1 km/s or 2.5 km/s V_S [1]. These models are referred to as ergodic [2], even if the site parameters are measured on site. The underlying models are ergodic because they are derived from large global or regional databases, and as such are not site-specific.

Any particular site would be expected to produce site amplification that departs from the ergodic estimate for a variety of reasons related to location-specific geologic conditions. A site amplification model that accounts for the effects of these features on site amplification is non-ergodic [e.g., 3]. One common feature of non-ergodic site response is resonance at one (fundamental site frequency, f_0) or more site frequencies (f_d) [4,5,6], which produce peaks that are smoothed out in ergodic models. The use of the horizontal-to-vertical Fourier amplitude spectral ratio (HVSR) vs. frequency plots have the potential to add this site-specific attribute to predictions of ergodic site response at low cost, relative to non-ergodic procedures. While V_{S30} provides a reasonable, first-order estimate of site response over a wide frequency range [7,8,9], f_0 can be effective at describing site amplification for frequencies proximate to f_0, but it has limited utility elsewhere. Hence, the two parameters serve different purposes and we postulate that they can be most effectively utilized together [10,11]. This paper concerns the development of a database to store HVSR data. The database stores HVSR data for the median component and for various horizontal azimuths, as-recorded signals in the time domain when not accessible from other data repositories, and the processing parameters used to derive the spectral ratios.

Many previous studies, mostly considering data from Europe, Japan, and central and eastern North America, have investigated the use of HVSR. These studies have generally found that HVSR is effective at identifying the peak frequency associated with resonance effects, whereas attempts to associate HVSR peak amplitudes with site amplification levels has been inconclusive [10,12,13,14,15].

This paper describes the extension of a V_S profile database (PDB), an early version of which is described by Ahdi et al. [16], to incorporate HVSR data. In this paper, we present a schema for the HVSR components of the database, where we explain the information that is stored and the results that can be readily extracted for ground motion studies. To place the schema in context, we explain the data acquisition process, the data processing procedures, procedures used to compute HVSR from the data, and external (to the database) routines that can be used to evaluate HVSR-related parameters used for site response studies.

2. Data Sources

The database is structured to allow entry of HVSR data from three sources: (1) microtremor array measurements (MAM) obtained from temporary deployments specifically targeting noise measurement [17, 21]; (2) three-component instruments installed temporarily or in permanent housings to record earthquakes but which also continuously stream microtremor data that is used for HVSR analysis; and (3) seismic signals [21]. A special case of Source 2 data is pre-event noise (microtremors immediately preceding an earthquake signal). Data from earthquakes, particularly when recorded by strong motion accelerometers, are typically from triggered instruments. Sources 1 and 2 are preferred because these match the data type that would generally be used in forward applications.

Comparisons of HVSR from seismograms (Source 3) to those from MAM (source 1) indicate that in many cases good matches are obtained [21,22]. However, the matches are not always favorable, and the conditions that give rise to poor matches are poorly understood. Figure 1 shows an example of HVSR data for a site in the California Bay-Delta region (YU_HOL2), including pre-event noise, an earthquake ("Seismic Event"), and MAM recordings. The MAM data indicates a peak frequency at about 4 Hz, whereas for other sources the frequency is lower and the peak amplitudes are reduced. As the database grows, we plan to investigate differences in HVSR from seismic and non-seismic signals for the same instrument, as well as differences in microtremor-based HVSR for different instrument types (seismometers and accelerometers).

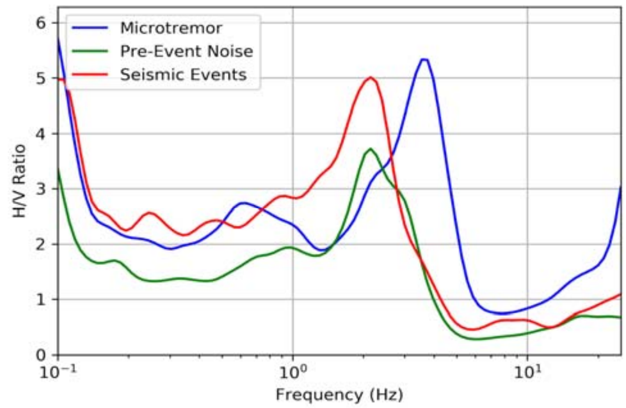

Figure 1 – Computed HVSR data from three sources for a site in the Delta (YU_HOL2): microtremor, pre-event noise, and seismic events.

While in California around 1,700 V_S profiles are publicly available via the PDB [16], fewer data exist for microtremor recordings. A major source of Source 1 HVSR data at strong motion stations is Yong et al. [17]. The study (aka: American Recovery and Reinvestment Act funded project; hereafter as ARRA project) presents data from 191 strong-motion stations, the majority of which are located in California (187 stations), with an additional four stations in the central and eastern United States. Additionally, we have Source 1 data from 33 sites in the Sacramento-San Joaquin Delta acquired by the 4th author. The California Strong Motion Instrumentation Program (CSMIP), part of the California Geological Survey (CGS), funded various studies to characterize ground motion recording station sites in California. A total of 12, 13, and 15 HVSR are available from the following CSMIP-funded reports: GEOVision [18], Petralogix [19], and GEOVision [20], respectively. These CSMIP reports have not yet been added to the database. Also included in the database is Source 2 data retrieved from the IRIS website for 831 sites with continuous-streaming high-gain seismometers and five sites with continuous-streaming accelerometers with sampling rates between 80-250 Hz. The five accelerometer sites are being considered in a trial study to compare HVSR from signals recorded by accelerometers to those obtained from seismometers. Figure 2 depicts the current site inventory in the database.

Using the data currently incorporated into the PDB, Figure 3 shows the relative number of V_S profiles and HVSR sites in California. Whereas various techniques have been used to collect profile data since the 1960s, the collection of microtremor data that is publicly accessible is much more recent. The sudden jump in microtremor data is from the present project, which is adding Source 2 data.

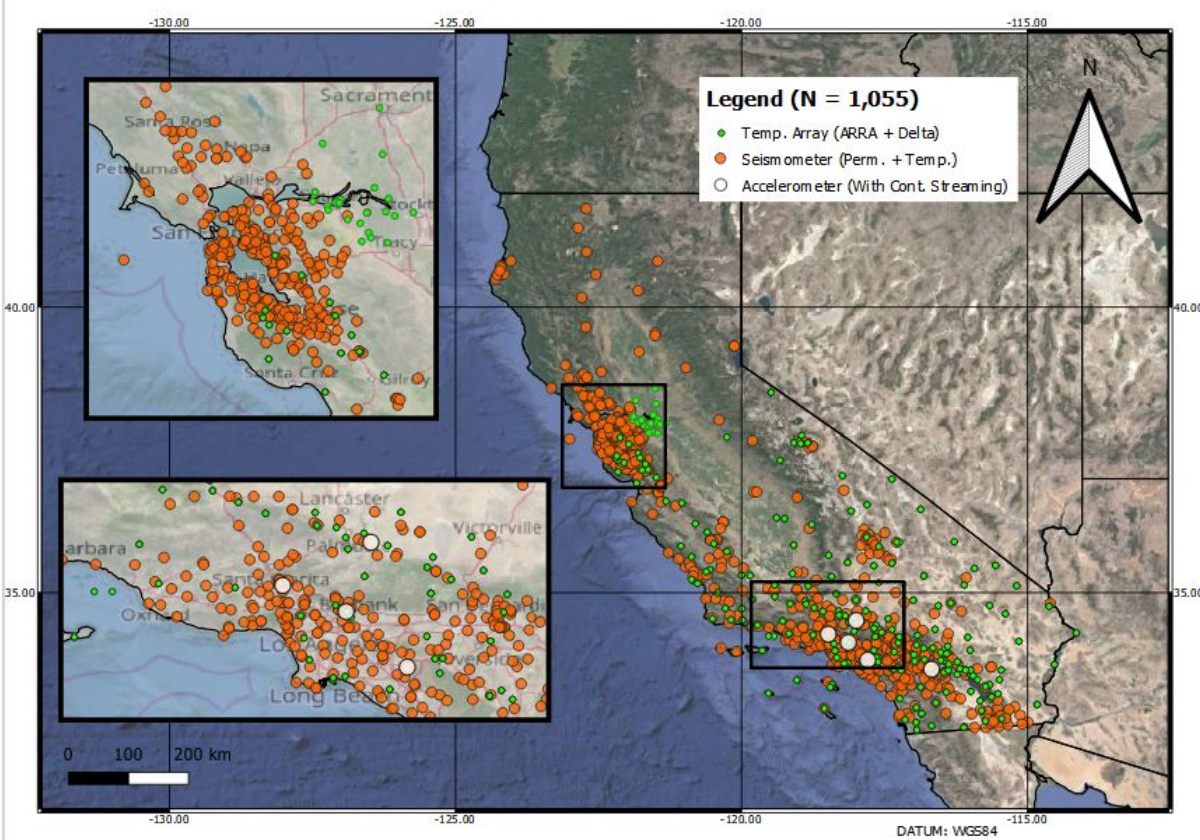

Figure 2 – Locations of sites in PDB with HVSR from either temporary deployments (MAM) or continuously streaming ground motion sensors (seismometers or accelerometers).

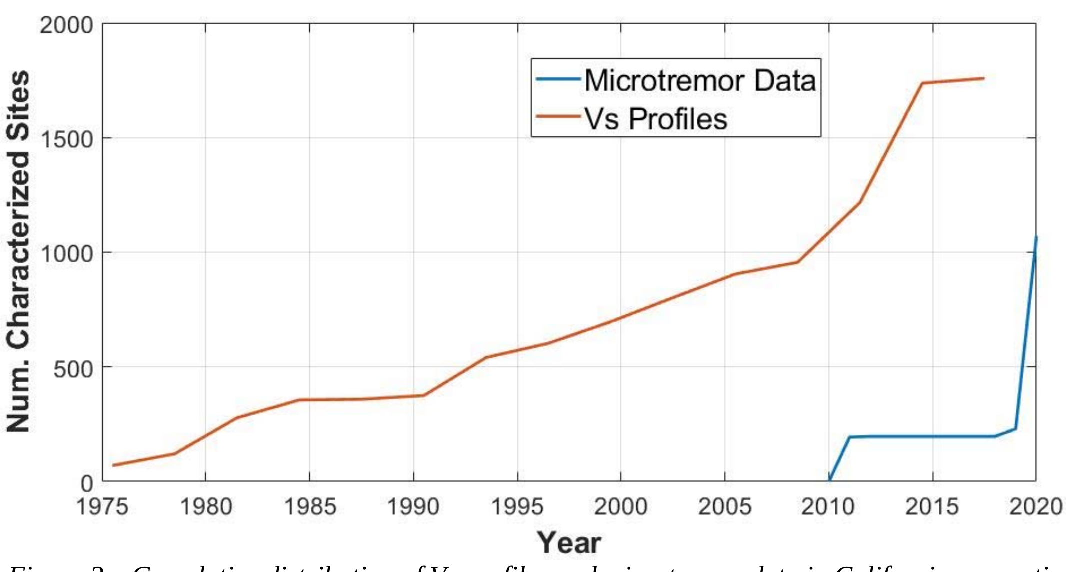

Figure 3 – Cumulative distribution of Vs profiles and microtremor data in California versus time.

3. Processing Parameters

This section describes the processing procedures that have been adopted to convert time-domain signals from triaxial seismometers or accelerometers to HVSR. These procedures borrow heavily from **S**ite **E**ffect**S** assessment using **AM**bient **E**xcitations (SESAME) guidelines [23] and protocols often used in California (K. Hayashi, A. Martin, oral and written personal communication, 2018, 2019). Signal processing has been performed using an HVSR processing code written in R by the 3rd author. In some cases (i.e., processing performed before that code was ready), the processing used Geopsy [24].

3.1 Microtremor Measurements

3.1.1 Number of Windows and Cycles

Data from Source types 1 or 2 in most cases consists of non-earthquake signals recorded over long durations (typically hours). The HVSR peak frequency should be greater than 10 divided by the window duration in seconds [23]. The total number of significant cycles is defined as $N_{cyc}=T_{win}\,f_0 N_{win}$, where T_{win} is window length (in sec), f_0 is the frequency (in Hz) of the lowest prominent peak in the H/V spectrum, and N_{win} is the number of windows used in the H/V spectrum computation. It is good practice to have no fewer than 200 cycles in the time series used for H/V computation, which effectively sets a minimum signal duration ($T_{sig} = N_{cyc} / f_0$).

Table 1 shows typical values for the above parameters as provided in recommendations for H/V testing in SESAME guidelines [23]. It is important to note that parameters can be manipulated to ensure that the number of significant cycles stays larger than 200.

Table 1 – Recommended recording duration, assuming at least N_{cyc} = 200 and N_{win} = 10 [23].

f_0 [Hz]	Minimum value for T_{win} [s]	Recommended minimum record duration T_{sig} [s]
0.2	50	1800
0.5	20	1200
1	10	600
2	5	300
5	5	180
10	5	120

3.1.2 Window Overlap; Taper Width and Type of Window

Sometimes the signal duration is not long enough and the windows may be too short in duration to satisfy the suggested window lengths (Table 1). To adjust for this, time windows can overlap by a specified percentage [24]. We use cosine tapers with a length of 5% of the window length [25].

3.1.3 Anti-Triggering

"Triggering" refers to a temporary vibration source affecting a signal, which can compromise the accuracy of HVSR. It is preferred for the ground vibrations producing the signals to be from far-field noise sources that produce approximately constant amplitudes in time. In contrast, local noise will have transient bursts due to the erratic nature of traffic or other anthropogenic sources. Anti-triggering is used on both the raw and filtered signal [23] to remove intervals of the signal with potential triggers. The objective of anti-triggering is to ensure approximately constant amplitudes in time.

The presence of potential triggers within a window of the recorded signal is judged based on relative values of the short-term average (STA) and long-term average (LTA) signal amplitudes. The STA and LTA are computed using 5- and 30-sec durations, respectively. The SESAME guidelines call for the amplitude ratios to be within the range of STA/LTA = 0.1 to 10 [23].

During signal processing, we look for stationary (i.e., approximately constant amplitude) intervals of ambient vibrations. Removing windows with transient signals produces clearer HVSR peaks and lowers dispersion. The anti-triggering algorithm is typically applied to both horizontal and vertical components.

While the anti-triggering algorithm can be applied to either the unfiltered or filtered noise signals, here we apply it to the raw (pre-filtered) signal (consistent with procedures used in Yong et al. [17]). Within the metadata table we provide STA duration, LTA duration, and the STA/LTA amplitude range.

3.1.4 Bad Sample Tolerance and Threshold

The bad sample tolerance and threshold options help the user optimize the number of windows [24]. The bad sample options allow windows to be selected that do not satisfy the anti-triggering criteria. The bad sample tolerance allows the user to define the number of bad samples which can remain in a usable window. The use of bad samples may be necessary if the available data do not allow the criteria in Table 1 to be met. Similarly, the bad sample threshold option allows the user to pick the total duration of bad signal in seconds that a window can have. The tolerance is expressed as a user-defined number of seconds, whereas the threshold is a percentage of the total points in a window.

3.1.5 Filter

Filtering is applied to reduce low-frequency drifts in waveforms. As such, software filtering is performed to cut low-frequency portions of signals. The corner frequency applied for this filter depends on the sensor used for analysis and is chosen manually for each signal. Given the equipment used in the field deployments described in Section 2, the corner frequency is usually around 0.1 Hz. The corner frequency for each signal is recorded as metadata. The upper bound frequency is determined by the Nyquist frequency. Theoretically, the application of filtering should not affect HVSR, since the same filter is applied to the horizontal and vertical components.

3.1.6 Smoothing Type and Constant

Spectral smoothing reduces high frequency noise and can facilitate identification of peaks. The Konno & Ohmachi [26] smoothing filter, which accounts for variable numbers of points at low frequency [23], is typically used and is applied to the combined horizontal and vertical components. We include different smoothing operators in the HVSR processing R code and the smoothing type is a field in the database discussed in Section 4.2. The degree of smoothing increases as the bandwidth decreases and smoothing is applied to the HVSR ratio for each window. Chatelain et al., [25] uses a bandwidth parameter of 40. We typically use a value of 30 and change this parameter depending on the quality of the data over the range of 20-40. Noisy data might need a lower bandwidth value.

3.1.7 Horizontal Component Combination Method

Because horizontal ground motions are recorded in two directions, a method to combine these components is required. The preferred method of horizontal combination is (1) median component (RotD50; Boore 2010), which mirrors applications in ground motion studies and (2) variable-azimuth components. The R code developed for this research provides this output. Geopsy version 3.2.1 does not provide these outputs, so for Geopsy-processed data the database stores the geometric mean.

3.1.8 HVSR Calculation

HVSR is computed as a function of frequency by dividing the smoothed RotD50 (or geometric mean) horizontal-component Fourier amplitudes by the smoothed vertical-component Fourier amplitudes. No further smoothing is applied to the ratio, other than through the averaging of results across windows. Section 5 describes routines that operate on information within the database to combine median-component HVSR and HVSR for various azimuths (every 10 degrees from true north to south). The uncertainties in HVSR ordinates are calculated as the standard deviation among the HVSR time windows.

3.2 Pre-event Noise

While ambient vibration recordings may be several hours long, pre-event noise is available in shorter durations for a particular record, and several such records may be available (one for each earthquake at the site). This is because pre-event noise is triggered data from strong motion stations, and these recordings ordinarily capture the seismic event and a few minutes of pre-event signal stored in instrument memory. Because of these differences in duration between pre-event noise and microtremor data, the processing steps discussed in Section 3.1 require modification. Here we present the main distinctions in HVSR analysis for pre-event noise.

We first obtain the data from a seismic ground motion data archive, such as IRIS [27]. Next, we identify the pre-event noise segment from each processed earthquake ground motion time series. Figure 4 illustrates the P-wave arrival and the selected window for HVSR analysis using pre-event noise. We identify the P-wave arrival time visually (Figure 4).

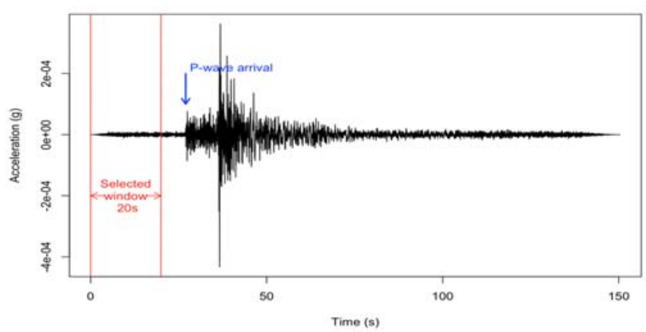

Figure 4 – Example of pre-event noise and P-wave arrival from IRIS earthquake strong motion data.

We repeat the above procedure for each available event at the site. Each event's pre-event noise is taken as the equivalent of a sub-window as used with MAM data processing. Per the SESAME guidelines in Table 1, ideally there would be at least 10 sub-windows (events), each with a minimum duration of 20 seconds (to resolve a peak frequency as low as 1 Hz). In practice, this is not always the case, which increases uncertainties in HVSRs evaluated using this method. After the time windows are selected, HVSRs are computed as described in Section 3.1.8. Uncertainties are also computed.

4. Database Schema

For the V_s profile database (PDB), a relational database was adopted as the means by which to organize and archive information [16]. This project adds HVSR to the PDB, which requires the addition of some tables to the existing database schema. The database has been developed using the My Structured Query Language (MySQL) relational database management system. Within the natural hazards community, there are many examples of "databases" that consist of non-structured data collections presented in the form of spreadsheets or text files. Structured relational databases represent a different tool to store data. Relational databases have a hierarchical structure that defines relationships among different tables. Data are stored in tables in a series of fields (or columns). The tables within the database are linked together through primary and foreign keys.

Primary keys represent unique identifiers of each entry in a table. Hence, one primary key can only be used once in each table. A foreign key is a field in one table used to identify a record in another table. Foreign keys are used to link different tables to each other. Relational databases were introduced by IBM employee E.F. Codd in 1970 [29], and some advantages include avoiding redundancy and null fields, consistency (information is entered only once), and security (if a database crashes, information is saved) [28,29].

The tables related to HVSR data in the PDB are listed in Table 2. There are two categories: general information and geophysical data. The meaning of the table names in Table 2 are described in subsequent subsections. Figure 5 shows all tables, specific fields, and the primary and foreign keys in each table.

Table 2 –Different group and table types and the number of fields in the HVSR schema.

Group Type	Table Type	No. Fields
General	site	18
	dataCitation	3
	citation	5
Geophysical	spectralRatioMeta	27
	hvProcessing	23
	meanCurve	5
	HV_Raw_FFT	9
	azimuthVariation	3
	polarCurve	4

4.1 Metadata

The purpose of the spectralRatioMeta table (Figure 5) is to provide the user with the processing parameters used to produce the HVSR curves. Some of these columns may be null depending on the source for the HVSR curve, which is noted in the last column, data_type of Figure 5. The primary key is the spectralRatioMeta_ID and the foreign key is the site_ID field.

4.2 Processing Table

The hvProcessing table provides the data processing parameters. The horizontal_combination field indicates if RotD50 or the geometric mean is used to combine the horizontal components. The smoothing_type indicates which smoothing operator is used. The primary key is the HV_Processing_ID and the foreign key spectralRatioMeta_ID.

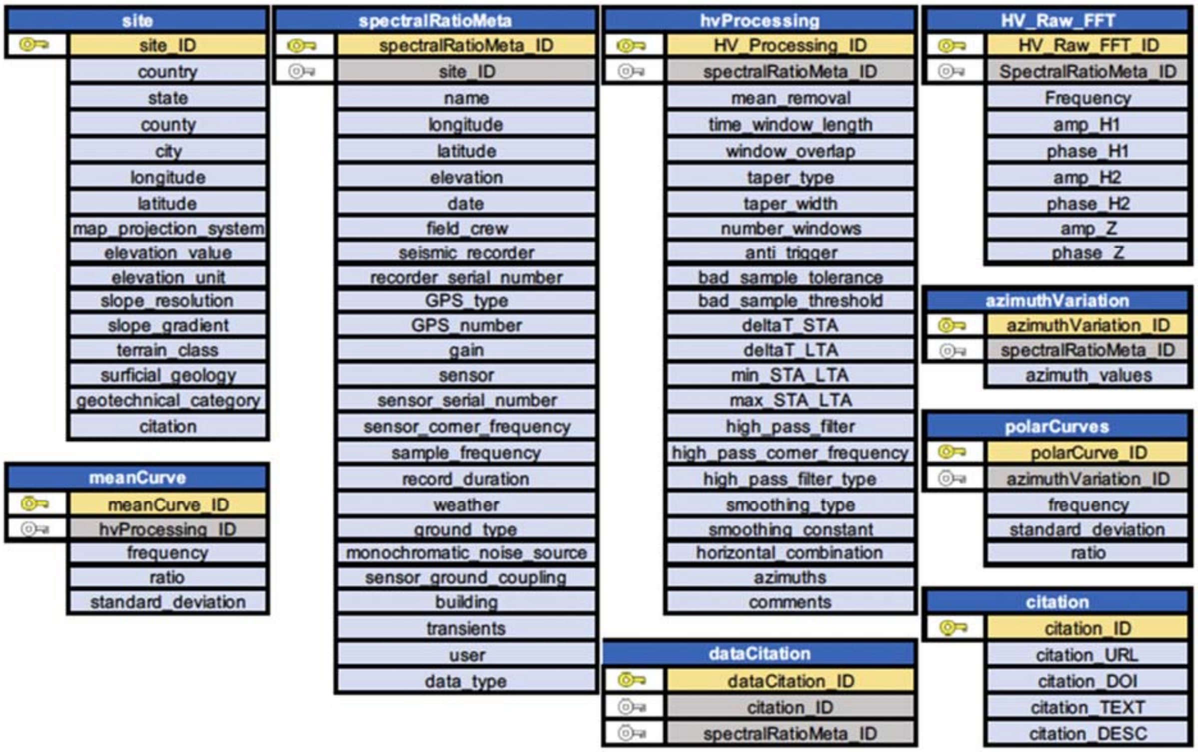

Figure 5 –Tables, fields, and primary (gold) and foreign (white) keys in HVSR database schema. Site table is taken from the V_S Profile Database schema developed by Ahdi et al. [30] and Sadiq et al. [31].

4.3 Raw Fourier Transform Curves

The HV_Raw_FFT_ID table stores the amplitude and phase data of the fourier transform from the time series for the two horizontal and vertical components. The primary key is the HV_Raw_FFT_ID and the foreign key spectralRatioMeta_ID.

4.4 Mean Curve Table

The meanCurve table provides the RotD50 or geometric mean HVSR ordinates averaged across all windows. The mean is computed for each frequency. The standard_deviation field is similarly computed using data from different time windows. For plotting purposes, we show the ratio of RotD50 or geometric mean HVSR and the mean +/- one standard_deviation (Figure 6). The primary key is the meanCurve_ID and the foreign key is hvProcessing_ID.

4.5 Azimuth Variation and Polar Curves Tables

The azimuthVariation includes azimuth values from 0 to 180 degrees in varying increments, typically around 5-10 degrees. The primary key and foreign key are the azimuthVariation_ID and spectralRatioMeta_ID, respectively. The polar curves table contains the curves (frequency, ratio, standard_deviation) for the azimuthVariation values where the polarCurve_ID is the primary key and the azimuthVariation_ID is the foreign key. Polar curves are generated by rotating the two horizontal components at selected azimuths. In the database, we typically store HVSR polar curves at 10-degree intervals (i.e. 18 polar curves - 0-180 degrees - for each site). The purpose of the polarCurve is to store HVSR data as a function of azimuth. Polar curves are often used to detect sites where topographic features may produce amplification effects due to wave-field polarization [32].

4.6 Data Citation and Citation Tables

The citation table provides storage to include URLs, DOIs, text, and descriptions related to the site. The primary key is citation_ID. The dataCitation table acts as a junction table between the citation and spectralRatioMeta table.

5. Tools for Data Interpretation Outside of Database

The PDB provides plots of RotD50 or geometric mean HVSR between time windows and tables showing azimuthal variations, but does not provide specific parameters derived from these results, such as might be used as site parameters to supplement V_{S30}. To facilitate such applications, the HVSR data archived in the relational database can be accessed via online Jupyter Notebook tools (example output in Figure 6). These tools interact with the data to interpret the data using protocols that have been applied in recent projects [3,31]. The interpreted parameters include (1) identification of features as peaks; (2) plots of azimuthal variations of HVSR; and (3) for each peak in the median-component HVSR, fitting of a pulse function to evaluate peak frequency, peak amplitude, and width of peak. We envision that such post-processing tools will be used to analyze the data in the cloud without the need to download data locally.

Figure 6 shows an example of a microtremor HVSR spectral ratio measurement in the Sacramento-San Joaquin Delta. Site CE_67265 is located under a bridge between two piers. The peak is dominated by the bridge response in the azimuthal variation plot around 0 or 180 degrees (N-S direction).

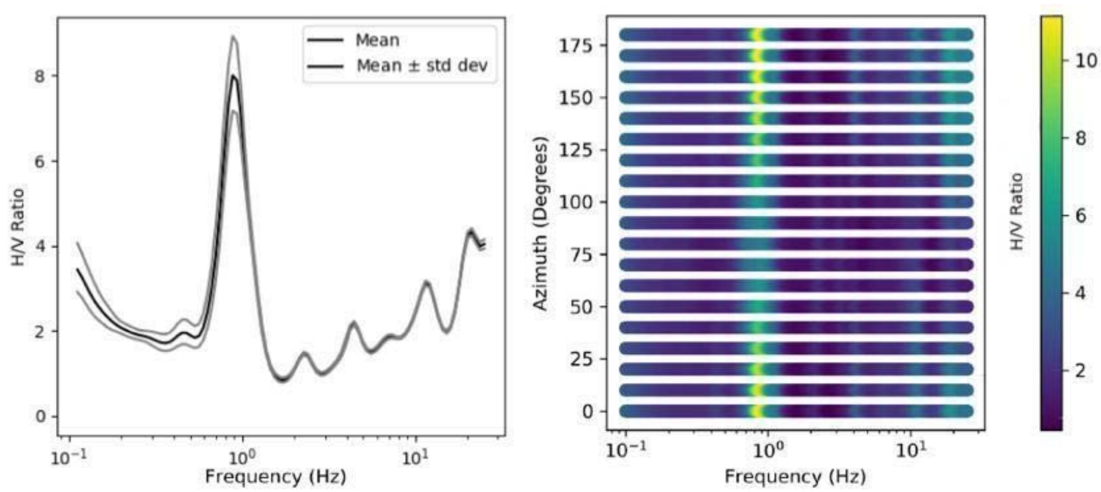

Figure 6 – A site in the Sacramento-San Joaquin Delta. Left:frequency versus H/V Ratio from a microtremor recording; right: azimuthal variation of the same recording.

HVSR plots can generally be classified as containing no peaks, one peak, or multiple peaks [12]. If there are multiple peaks, we take the first two peaks (i.e., the two peaks at the lowest frequencies). A peak generally indicates the site has strong impedance contrast(s) near one or more modal frequencies [e.g., 33] whereas multiple peaks may indicate multiple impedance contrasts at different depths. When there is no peak present in an HVSR, this suggests the site is either underlain with a sediment-filled depth profile that lacks a significant impedance contrast or it is a rock site with nearly depth-invariant near-surface velocities.

Peak identification occurs in two steps. In the first step, a visual check is performed to evaluate if the peak amplitude exceeds the maximum of 2.0 or 1.5×the mean amplitude over the usable frequency range [34]. The second step is based on the "second criteria" of [23; page 10] for identification of reliable and clear peaks. The details of this procedure are omitted for brevity. For mean HVSR plots with a peak, we fit a Gaussian pulse function defined as follows:

$$\hat{F}_{HV,i} = c_0 + c_i \exp\left(-\frac{1}{2}\left(\frac{ln(f/f_{pi})}{2w_i}\right)^2\right) \tag{1}$$

where f_{pi} is the fitted peak frequency, c_i is peak amplitude, w_i is peak width, i is the order of peak, c_0 is a frequency-independent constant, and f is frequency in Hz. This Gaussian pulse function estimates a pulse amplitude, frequency, and width for each peak. The nonlinear regression is performed in R using the Optim function by minimizing the sum of squared errors. Figure 7 shows results for two example sites. The site in Part (a) has local maxima, but they are too small in amplitude and width to be considered as peaks. The site in Part (b) contains a peak at 0.3 Hz, which is fit using the above Gaussian function.

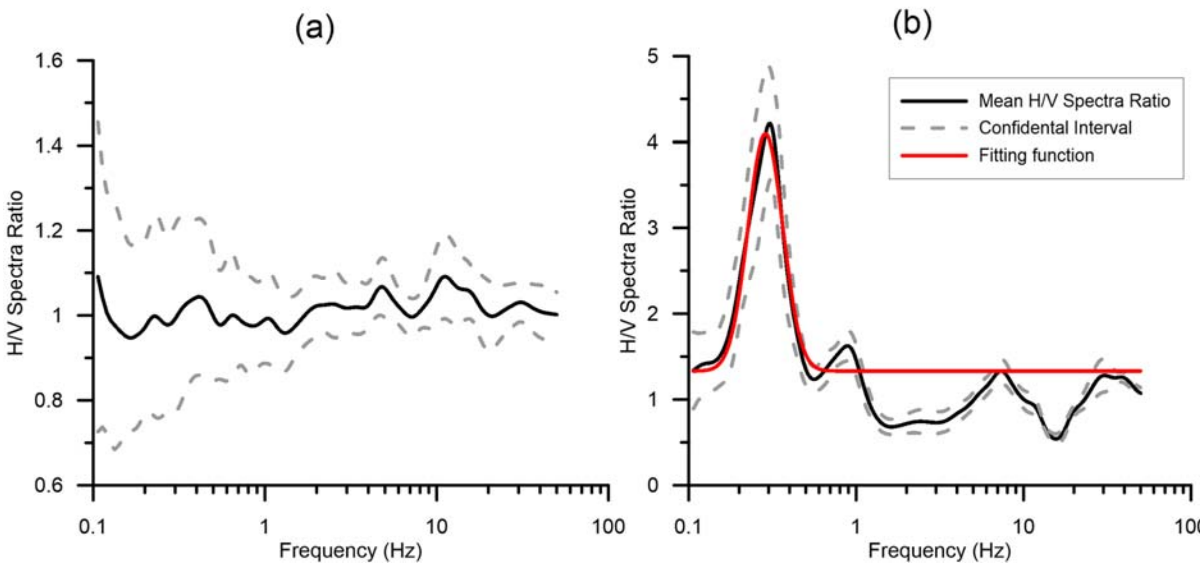

Figure 7 – RotD50 HVSR for two example sites in California. (a) site without an identified peak; (b) site with single peak and Gaussian fit to the peak using Eq. (1).

6. Conclusions

We created an open-source relational database of HVSR and associated processing parameters and incorporate this information into an existing community V_s Profile Database (PDB) in the United States. Users can utilize and analyze the processed records through interactive Jupyter Notebook tools. The addition of the H/V site parameter is a valuable resource for future studies and will pave the way for HVSR-based parameters to be included in the site database used in future NGA-type ground motion model development projects. We anticipate that this data will also prove useful over time for site-specific ground motion studies in the US.

7. Acknowledgments

Funding for this study is provided by California Strong Motion Instrumentation Program, California Geological Survey, Agreement 1016-985 and 1018-569. We gratefully acknowledge this support. We also thank Antony Martin from GEOVision for sharing his expertise on processing the HVSR data. We thank Silvia Castellaro, Seth Carpenter, Brady Cox, Hiroshi Kawase, Shinichi Matsushima, Stefano Parolai, Marco Pilz, Lisa Schleicher, Jamison Steidl, and Wang Zhenming for their input on this paper. Any use of trade, firm, or product names is for descriptive purposes only and does not imply endorsement by the U.S. Government.

8. References

[1] Bozorgnia, Y., N. A. Abrahamson, L. .A. Atik, T. D. Ancheta, G. M. Atkinson, J. W. Baker, A. Baltay, D. M. Boore, K. W. Campbell, B. S.-J. Chiou, R. Darragh, S. Day, J. Donahue, R. W. Graves, N. Gregor, T. Hanks, I. M. Idriss, R. Kamai, T. Kishida, A. Kottke, S. A. Mahin, S. Rezaeian, B. Rowshandel, E. Seyhan, S. Shahi, T. Shantz, W. Silva, P. Spudich, J. P. Stewart, J. Watson-Lamprey, K. Wooddell, and R. Youngs, 2014. NGA-West 2 research project, *Earthq. Spectra*, **30**, 973-987.

[2] Anderson, J. G. and J. Brune, 1999. Probabilistic seismic hazard analysis without the ergodic assumption." *Seism. Res. Lett.*, **70**, 19-28.

[3] Stewart, J. P., K. Afshari, and C. A. Goulet, 2017. Non-ergodic site response in seismic hazard analysis, *Earthq, Spectra*, **33**, 1385-1414.

[4] Di Alessandro, C., L. F. Bonilla, D. M. Boore, A. Rovelli, and O. Scotti, 2012. Predominant-period site classification for response spectra prediction equations in Italy, *Bull. Seismol. Soc. Am.* **102**, 680–695.

[5] Bonilla, L.F., J. H. Steidl, J.-C. Gariel, and R.J. Archuleta (2002). Borehole response studies at the Garner Valley downhole array, Southern California, *Bull. Seismol. Soc. Am.* **92,** 3165-3179.

[6] Bonilla, L. F., J. H. Steidl, G. T. Lindley, A. G. Tumarkin, and R. J. Archuleta (1997). Site amplification in the San Fernando Valley, California: Variability of site-effect estimation using the S-wave, coda, and H/V methods, *Bull. Seismol. Soc. Am.* **87,** 710-730.

[7] Abrahamson, N. A., W. J. Silva, and R. Kamai (2014). Summary of the ASK14 ground motion relation for active crustal regions, *Earthq. Spectra* **30,** 1025-1055.

[8] Campbell, K. W., and Y. Bozorgnia (2014). NGA-West2 ground motion model for the average horizontal components of PGA, PGV, and 5% damped linear acceleration response spectra, *Earthq. Spectra* **30,** 1087-1115.

[9] Chiou, B. S.-J., and R. R. Youngs (2014). Update of the Chiou and Youngs NGA model for the average horizontal component of peak ground motion and response spectra, *Earthq. Spectra* **30,** 1117-11153.

[10] Cadet, H., P.-Y. Bard, A.-M. Duval, and E. Bertrand (2012). Site effect assessment using KiK-net data: Part 2—Site amplification prediction equation based on f0 and Vsz, Bull. Earthq. Eng. 10, 451–489.

[11] Gofrani, H., G.M. Atkinson, and K.Goda (2013). Implications of the 2011 M 9.0 Tohoku Japan earthquake for the treatment of site effects in large earthquakes, *Bull. Earthq. Eng.* **11,** 171-203.

[12] Kwak, D. Y., Stewart, J. P., Mandokhail, S. U. J., and Park, D. (2017). Supplementing VS 30 with H/V spectral ratios for predicting site effects. *Bull. Seismol. Soc. Am.* **107**, 2028-2042.

[13] Field, E. H., and K. H. Jacob (1993). The theoretical response of sedimentary layers to ambient seismic noise, *Geophys. Res. Lett.* **20**, 2925–2928.

[14] Theodulidis, N., R. J. Archuleta, P.-Y. Bard, and M. Bouchon (1996). Horizontal to vertical spectral ratio and geological conditions: The case of Garner Valley downhole array in southern California, *Bull. Seismol. Soc. Am.* **86**, 306–319.

[15] Kawase, H., Mori, Y., and Nagashima F. (2018). Difference of horizontal-to-vertical spectral ratios of observed earthquakes and microtremors and its application to S-wave velocity inversion based on the diffuse field concept. *Earth, Planets and Space*, **70**, 1.

[16] Ahdi, S.K., O. Ilhan, S. Sadiq, Y. Bozorgnia, Y.M.A. Hashash, D. Park, A. Yong, and J.P. Stewart (2018). Development of a United States Community Shear Wave Velocity Profile Database, *5th Conference on Geotechnical Earthquake Engineering and Soil Dynamics (GEESD-V)*, June 10–13, 2018, Austin, Texas.

[17] Yong, A, A Martin, KH Stokoe, and J Diehl, 2013, ARRA-funded VS30 measurements using multi-technique approach at strong-motion stations in California and central-eastern United States: U.S. Geological Survey Open-File Report 2013–1102, 59 p. and data files, http://pubs.usgs.gov/of/2013/1102/.

[18] GEOVision (2016). Surface Wave Measurements Report, Riverside County, California. Report 16192-01 Rev 2. Prepared for State of California Department of Conservation, California Geological Survey, Strong Motion Instrumentation Program.
[19] Petralogix (2017). Vs30 Site Characterization Report, Los Angeles, Orange, Ventura, San Bernardino, and Riverside Counties. Report 2017-00006.
[20] GEOVision (2018). Surface Wave Measurements, Santa Clara, Santa Cruz, San Benito, and Monterey Counties. Report 18045-01. Prepared for State of California Department of Conservation, California Geological Survey, Strong Motion Instrumentation Program.
[21] Hassani, B., Yong, A., Atkinson, G. M., Feng, T., and Meng, L. (2019). Comparison of site dominant frequency from earthquake and microseismic data in California. *Bull. Seismol. Soc. Am.*, **109(3),** 1034-1040.
[22] Satoh, T., H. Kawase, and S. Matsushima (2001). Differences between site characteristics obtained from microtremors, S-waves, P-waves, and codas, *Bull. Seismol. Soc. Am.* **91**, 313–334.
[23] SESAME, 2004, Guidelines for the Implementation of the H/V spectral ratio technique on ambient vibrations—Measurements, processing and interpretation: European Commission, Project No. EVG1-CT-2000-00026, accessed September 2012, at http://sesame-fp5.obs.ujf-grenoble.fr/
[24] Wathelet M. (2006). Geopsy Manual.
[25] Chatelain, J.-L., B. Guillier, B., Cara, F., Duval, A.-M., Atakan, K., Bard, P.-Y., and The WP02 SESAME team, (2008). Evaluation of the influence of experimental conditions on H/V results from ambient noise recordings, *Bull. Earthq. Eng,* **6**, 33–74.
[26] Konno, K., and Ohmachi, T. (1998). Ground-motion characteristics estimated from spectral ratio between horizontal and vertical components of microtremor. *Bull. Seismol. Soc. Am.* **88(1),** 228-241.
[27] "Incorporated Research Institutions for Seismology (IRIS), IRIS Earthquake Browser, http://ds.iris.edu/ieb/index.html, last accessed <01/07/2019>
[28] Brandenberg S.J., Zimmaro P., Stewart J.P., Kwak D.Y., Franke K.W., Moss R.E.S., Cetin K.O., Can G., Ilgac M., Stamatakos J., Weaver T., and Kramer S.L. (2019). Next Generation Liquefaction Database. *Earthq. Spectra*. In Press. DOI: 10.1177/8755293020902477.
[29] Codd, E. F. (1970). A relational model of data for large shared data banks. *Communications of the ACM*, *13*(6), 377-387.
[30] Ahdi, S. K. (2018). An Improved Framework for the Analysis and Dissemination of Seismic Site Characterization Data at Varying Resolutions. *UCLA*. ProQuest ID: Ahdi_ucla_0031D_17519. Merritt ID: ark:/13030/m54f6nxb. Retrieved from https://escholarship.org/uc/item/6p35w167
[31] Sadiq, S., O. Ilhan, S.K. Ahdi, Y. Bozorgnia, Y.M.A. Hashash, D. Park, A. Yong, and J.P. Stewart (2018). A Proposed Seismic Velocity Profile Database Model. *Eleventh U.S. National Conference on Earthquake Engineering (11NCEE)*, June 25–29, 2018, Los Angeles, California, Paper No. 1342.
[32] Di Giulio G., Cara F., Rovelli A., Lombardo G., and Rigano R. (2009). Evidences for strong directional resonances in intensely deformed zones of the Pernicana fault, Mount Etna, Italy. *Journal of Geophysical Research*, **114**, B10308.
[33] Tuan, T. T., F. Scherbaum, and P. G. Malischewsky (2011). On the relationship of peaks and troughs of the ellipticity (H/V) of Rayleigh waves and the transmission response of single layer over half-space models, *Geophys. J. Int*. **184**, 793–800.
[34] Hassani, B and GM Atkinson, 2016. Applicability of the site fundamental frequency as a V_{S30} proxy for Central and Eastern North America, *Bull. Seismol. Soc. Am.* **106**, 653–664.